CrossMark

Structure, microstructure and physicochemical properties of $BaW_{1-x}Nb_xO_{4-\delta}$ materials

Agnieszka Lacz[1] · Barbara Bak[1] · Radoslaw Lach[1]

Abstract

Nb-doped $BaWO_4$ with the assumed formula $BaW_{1-x}Nb_xO_{4-\delta}$ ($x = 0$, 0.005, 0.01, 0.02 and 0.05) were prepared by solid-state reaction method. Crystal structure and phase composition were determined by X-ray diffraction method. Scanning electron microscopy (SEM) coupled with energy-dispersive spectrometry (EDS) was used to describe microstructure and chemical composition of synthesised materials. It was found that solubility limit of niobium in the $BaWO_4$ structure is the range 0.5–1 mol%, as formation of second phase—$Ba_5Nb_4O_{15}$—was observed for samples with higher dopant content. For evaluation of the chemical stability of synthesized materials, the comparative CO_2/H_2O exposure test was performed. Samples were exposed to carbon dioxide- and water vapour-rich atmosphere (7% CO_2 in air, 100% RH) at 298 K for 700 h. During this exposition, the chemical reactions between the samples and the surrounding gaseous atmosphere resulting in formation of barium hydroxide and/or barium carbonate can process. Thermogravimetry (TG) method was used for chemical stability evaluation. The comparison of samples before and after the CO_2/H_2O exposure test was performed. To support the interpretation of TG results, the analysis of gaseous products evolved during thermal treatment of the samples was done using mass spectrometer. The effect of dopant on the $BaWO_4$ chemical stability improvement was observed. In order to determine the electrical properties of obtained materials, the DC resistance measurements in synthetic air atmosphere were taken. It was shown that niobium doping and the presence of second phase—$Ba_5Nb_4O_{15}$—leads to an increase in the total conductivity of synthesised materials.

Keywords Scheelite structure · Barium tungstate · Niobium-doped $BaWO_4$ · Chemical stability

Introduction

Materials with general formula ABO_4 (where $A = $ Ba, Sr, Pb and $B = $ W or Mo) and scheelite-type structure are considered as perspective for optical and electronic applications, e.g. phosphors, optical fibres, catalysts, laser host materials, scintillator detectors [1–6]. Wide range of synthesis method was applied to received ABO_4 materials, for example solid-state reaction [7], sol–gel [8], co-precipitation [9], hydrothermal [10, 11], microwave-assisted [12, 13] or sonochemical [14]. Synthesis of doped materials, like calcium- or lead-doped $SrWO_4$, tungsten-doped $SrMoO_4$, terbium- or strontium-doped $BaWO_4$, are mainly focused on potential optical applications [15–19]. Doping of scheelite-type structure materials (e.g. $BaWO_4$, $SrWO_4$, $PbWO_4$) towards improvement in their electrical properties is not widely discussed, and this field of scientist research is quite open. It is well known that chemical and thermal stability of tungstates with scheelite structure is high [20, 21]. According to the literature, introduction of $BaWO_4$ as the second phase into the Y-doped $BaCeO_{3-\delta}$ materials leads to an increase in the CO_2 resistance but simultaneously the electrical conductivity decreases [22]. It is also known that conductivity of acceptor-doped $BaWO_4$ is protonic [23] and the electrical conductivity of the scheelite-type structure $SrWO_4$ depends on the oxygen partial pressure what allows to classify strontium tungstate as the p-type conductor [24]. It should be mentioned that doping of ABO_4 structure reported in the literature considers mainly the substitution in the A position [25–27].

✉ Agnieszka Lacz
  alacz@agh.edu.pl

[1] Faculty of Materials Science and Ceramics, AGH University of Science and Technology, al. A. Mickiewicza 30, 30-059 Krakow, Poland

Incorporation of samarium or lanthanum into lead position in $PbWO_4$ results in an increase in total conductivity [26], similarly as doping of $BaWO_4$ with cesium or strontium [19, 27] and incorporation of lanthanum into $CaWO_4$ structure [28]. Significant value of ionic conductivity was reported for scheelite-type structure $A_{1-x}Li_{2x}BO_4$ (A = Ca, Sr, Ba, B = W, Mo) compounds [25]. Recently, the proton conductivity was reported for $CaW_{1-x}Ta_xO_{4-\delta}$ materials; however, the solubility limit of thallium in $CaWO_4$ structure was lower than 1 mol% [29]. Nevertheless, the literature concerning electrical properties of tungstates with general formula AWO_4 is rather marginal though it implies they are perspective materials.

In this work, introduction of acceptor dopant (niobium) to the $BaWO_4$ scheelite-type structure into tungsten position was assumed. To our knowledge, this type of barium tungstate modification was not studied previously. The purpose of this work was to determine the solubility limit of niobium in the $BaWO_4$ structure while materials are synthesised by solid-state reaction and to discuss the effect of dopant on the microstructure and the stability of $BaW_{1-x}Nb_xO_4$ materials towards CO_2 and water vapour at low-temperature exposure along with the analysis of the electrical properties of pure and doped barium tungstate.

Experimental

Samples of Nb-doped $BaWO_4$ with the general formula $BaW_{1-x}Nb_xO_{4-\delta}$ (with x = 0, 0.005, 0.01, 0.02 and 0.05) were synthesised by solid-state reaction method. Barium carbonate $BaCO_3$ and tungsten and niobium oxides (WO_3 and orthorhombic Nb_2O_5), all with analytical grade supplied by Sigma-Aldrich Chemical Company Inc, were used. The precursor's mixtures were formed in the pallet dies and calcined at 1223 K for 24 h in the 1.5 dm^3 min^{-1} air flow. The calcination conditions were optimized basing on TG and DTA results (SDT 2960 TA Instruments, mass about 50 mg, heating rate 10 K min^{-1}, synthetic air atmosphere, platinum crucibles) and XRD analysis. Received materials were crushed, milled in absolute alcohol suspension (ZrO_2 grinding media) and after drying (363 K for 24 h) again formed in a pellet dies, isostatically pressed (250 MPa) and sintered at 1573 K for 3 h in air atmosphere. The samples diameter before sintering was 9.50–9.60 mm; after sintering, the diameter decreases as the shrinkage of the samples was observed. The difference in the shrinkage ability was observed for un-doped $BaWO_4$ and Nb-doped $BaWO_4$. For un-doped material, the average diameter after sintering was 9.25 mm; for Nb-doped samples, the average diameter 9.05–9.15 mm was measured.

In the following part of the paper, the samples with the assumed composition $BaW_{1-x}Nb_xO_{4-\delta}$ (x = 0, 0.005, 0.01, 0.02 and 0.05) will be labelled as: $BaWO_4$, 0.5Nb_$BaWO_4$, 1Nb_$BaWO_4$, 2Nb_$BaWO_4$ and 5Nb_$BaWO_4$, respectively.

To define the phase composition and crystal structure of sintered $BaW_{1-x}Nb_xO_{4-\delta}$ materials, the X-ray diffractometer Philips X'Pert (monochromatized CuKα radiation) was used. Rietveld phase analysis was applied to determine the amounts of observed phases and crystallographic parameters. Microstructure and chemical composition were verified by scanning electron microscopy SEM (Nova Nano SEM 200 FEI & Oxford Instruments) combined with energy-dispersive spectrometry (EDS) (FEI & Oxford Instruments). The total porosity of samples was determined on the basis of sample mass and geometry.

To evaluate the chemical stability of the samples for CO_2 and H_2O, the exposure test was performed. Samples were exposed to carbon dioxide- and water vapour-containing atmosphere (7% CO_2 in air, 100% RH) at 298 K for 700 h. Thermal analysis combined with mass spectrometry was applied to analyse the results of the exposure test. All samples before and after the exposition were heating in the SDT 2960 TA Instruments apparatus (synthetic air flow, mass of samples 50 mg, heating rate 10 K min^{-1}) coupled with the mass spectrometer QMD300 ThermoStar Balzers to identify the evolved gaseous products.

The electrical properties were determined based on DC resistance measurements. The temperature variation resistance measurement was taken by Keysight Technology multimeter in fully automatic system using two-probe method. The measurements were taken on sintered pellets in the form on discs (about 9 mm in diameter and 4 mm of thickness) as a function of temperature (798–973 K) for synthetic air. Samples were equilibrated for 30 min at the specific temperature before each measurement. For each temperature, nine resistance measurements were taken. The conductivity was calculated based on measured resistance and sample geometry.

Results and discussion

Phase composition, structure and microstructure

Based on the XRD results, the phase composition and crystal structure of Nb-doped $BaWO_4$ materials were determined. For $BaWO_4$, 0.5Nb_$BaWO_4$ and 1Nb_$BaWO_4$ samples, single-phase scheelite-type structure material was found, described as tetragonal (space group I41/a, ICSD No. 01-085-0588). For two others, 2Nb_$BaWO_4$ and 5Nb_$BaWO_4$, the second phase—hexagonal $Ba_5Nb_4O_{15}$ (ICSD No. 98-009-5192)—was also identified (Fig. 1).

The amount of $Ba_5Nb_4O_{15}$ estimated by the Rietveld method was around 1.6 and 5.7 mass% for 2Nb_$BaWO_4$

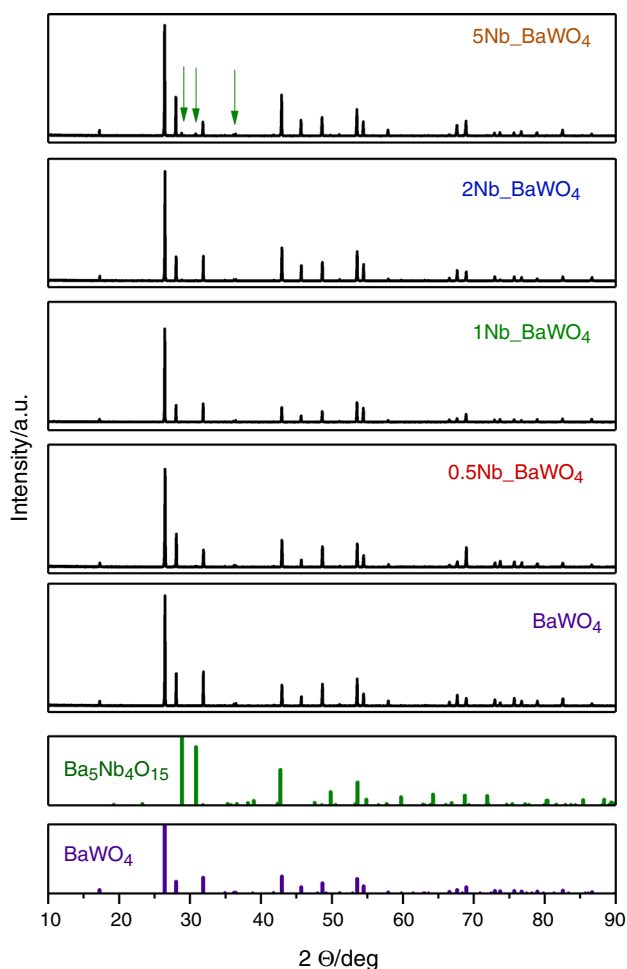**Fig. 1** X-ray diffraction pattern of $BaWO_4$ and Nb-doped $BaWO_4$ sintered samples

tungsten position should lead to a slight increase in the unit cells parameters. The data collected in Table 1 show that changes in the lattice parameters are small. The increase in lattice parameter is clearly seen only for sample with the smallest dopant amount (0.5Nb_BaWO_4) and suggests that 0.5 mol% of niobium can be incorporated into tungsten position in $BaWO_4$ structure. The sample label as 1Nb_BaWO_4 is a little concerning. The analysis performed by Rietveld method suggests that material with 1 mol% of niobium is single phase, and niobium was totally incorporated into $BaWO_4$ structure. The values of lattice parameters do not follow this thought; they should be higher than for $BaWO_4$ and 0.5Nb_BaWO_4. It strongly suggests that 1Nb_BaWO_4 material is not single phase, and the amount of second phase was below the detection point of XRD method or the $Ba_5Nb_4O_{15}$ phase was amorphous. Thus, it can be concluded that the solubility limit of niobium in the $BaWO_4$ structure is in the range 0.5–1 mol%. For regular two-phase materials (2Nb_BaWO_4 and 5Nb_BaWO_4), the lattice parameters are comparable with lattice parameters of un-doped $BaWO_4$. However, it should be noticed that partial incorporation of niobium into $BaWO_4$ structure for not single-phase materials cannot be excluded. In particular, that slight increase in the cell volume of $BaWO_4$ for materials with introduced niobium was observed (Table 1). This effect can be the result of incorporation of larger cation (Nb^{5+}) into $BaWO_4$ structure.

SEM microphotographs together with the EDS spectrum for the sample with the highest niobium content are presented in Fig. 2. For all materials, regardless of the chemical composition, the grain size is 20–50 μm and grains elongation is clearly visible. The crystallite sizes, estimated for all samples based on peak width at half-height, were in the range 90–120 nm without any trend related to the amount of introduced niobium. It indicates that each grain is composed of several crystallites. The cracks observed on the SEM microphotographs occur possibly during cooling of sintered samples and probably are the results of high anisotropy of $BaWO_4$ thermal expansion coefficient $10.9 \cdot 10^{-6} \times 10.8 \cdot 10^{-6} \times 35 \cdot 10^{-6}$ K^{-1} [31]. The samples mass and geometry (diameter and thickness) together with the theoretical density (for

and 5Nb_BaWO_4 samples, respectively (Table 1). It suggests that the solubility limit of niobium incorporated into tungsten position in the $BaWO_4$ structure is between 1 and 2 mol%. This could be verified by analysis of the unit cells parameters of tetragonal $BaWO_4$ as a function of introduced niobium (Table 1).

In the ABO_4 scheelite-type structure, the coordination number (CN) is 8 and 4 for A and B cation, respectively. The ionic radius of W^{6+} for CN = 4 is 0.42 Å and is only slightly lower than ionic radius of Nb^{5+} (0.48 Å for CN = 4) [30]. Thus, incorporation of niobium into

Table 1 $BaWO_4$ lattice parameters, cell volume and determined phase composition of synthesized materials

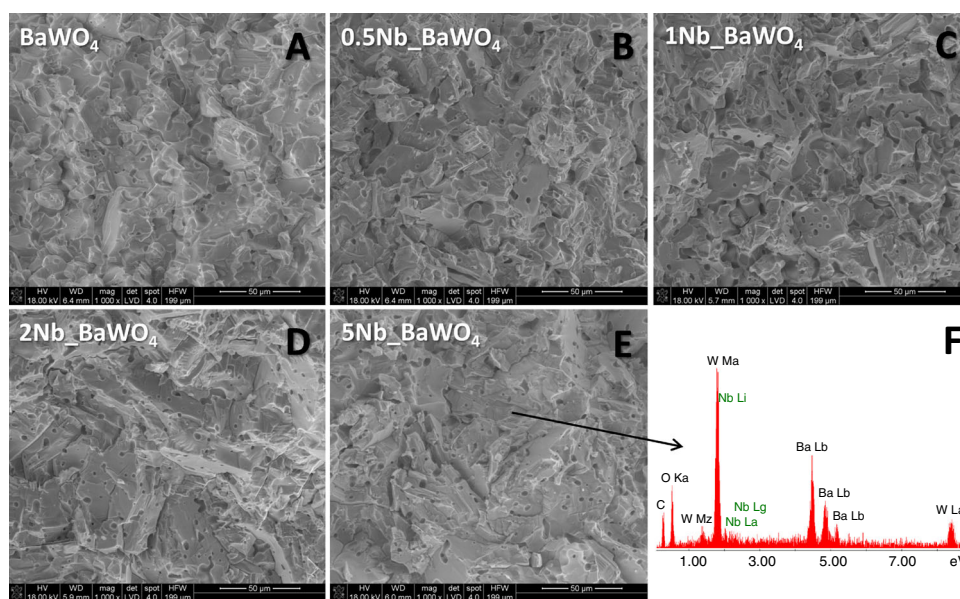|	a/Å in $BaWO_4$	c/Å in $BaWO_4$	V/Å³	$BaWO_4$/mass%	$Ba_5Nb_4O_{15}$/mass%
$BaWO_4$	5.6161 ± 0.0006	12.7267 ± 0.0008	401.41	100	
0.5Nb_BaWO_4	5.6171 ± 0.0005	12.7295 ± 0.0011	401.64	100	
1Nb_BaWO_4	5.6169 ± 0.0009	12.7262 ± 0.0009	401.54	100	
2Nb_BaWO_4	5.6163 ± 0.0005	12.7284 ± 0.0011	401.49	98.4	1.6
5Nb_BaWO_4	5.6161 ± 0.0004	12.7266 ± 0.0009	401.40	94.3	5.7

Fig. 2 SEM microphotographs of $BaWO_4$-based samples (**a**–**e**) together with the results of EDS analysis of $5Nb\_BaWO_4$ sample (**f**)

tetragonal $BaWO_4$ 6.38 g cm^{-1} from ICSD Card No. 01-085-0588) were used to determine the samples total porosity. For un-doped $BaWO_4$, total porosity was about 20%; for niobium-doped samples, this value was slightly smaller and reached 12–15%. SEM microphotographs clearly show high content of close porosity for all materials. To calculate the volume fraction of close porosity, the stereology can be applied [32]. For single-phase materials, the estimated fraction of close porosity was 19% and 13–15% for $BaWO_4$ and single-phase Nb-doped $BaWO_4$, respectively, and was close to the determined total porosity. For two-phase materials, $2Nb\_BaWO_4$ and $5Nb\_BaWO_4$, volume fraction of close porosity was smaller and reached 10 and 8%, respectively. It can suggest that the presence of the second phase ($Ba_5Nb_4O_{15}$) improves the materials sinterability.

Chemical stability

Chemical stability of materials with potential applications in electrochemical devices is one of the crucial parameters. Chemical instability results mainly in deterioration of electrical and mechanical properties. For that reason, chemical stability test (long-term, low-temperature exposure to CO_2 and water vapour) simulating the materials storage conditions was performed for all synthesised materials. During this exposition the adsorption of water and/or CO_2 can process and/or the chemical reactions between the samples and the surrounding gaseous atmosphere rich with water vapour and carbon dioxide. It can result in formation of barium hydroxide and/or barium carbonate. Thus, after the exposure test the phase

composition of sample can be different than before the exposition to CO_2 and water vapour.

Thermal analysis combined with mass spectrometry was applied for evaluation of the chemical stability. Thermogravimetry curves (TG) together with the $m/z = 18$ and $m/z = 44$ ion current lines were collected for all tested samples. The lines for $m/z = 18$ and $m/z = 44$ illustrate the evolving of water and carbon dioxide—the potential gaseous product of thermal degradation of samples before and after the exposition test.

In Fig. 3, TG curves together with the $m/z = 18$ and $m/z = 44$ ion current lines for thermal degradation of un-doped $BaWO_4$ sample before and after the exposition test are presented. For sample before the test, the total mass loss is about 0.02% and the only effect clearly visible on TG curve is observed below the temperature 673 K and is the result of elimination of water from the sample. After the test, additional effects are seen, leading to the total mass loss about 0.09%. The two steps of degradation between the temperature ranges 873–1173 K can be observed; both are connected with evolving of CO_2; thus, both steps can be described as decomposition of $BaCO_3$ formed during the exposition test. As it is reported in the literature, the temperature of barium carbonate decomposition is about 1173 K, however, strongly depending on the surrounding atmosphere [33]. The two steps of decomposition can suggest that $BaCO_3$ formed during the exposition can be partially amorphous, as the decomposition temperature of non-crystalline and crystalline barium carbonate can be different. The content of $BaCO_3$ in the initial sample, calculated based on the mass loss, is about 0.15%. The mass loss calculated based on the TG curve for the first and
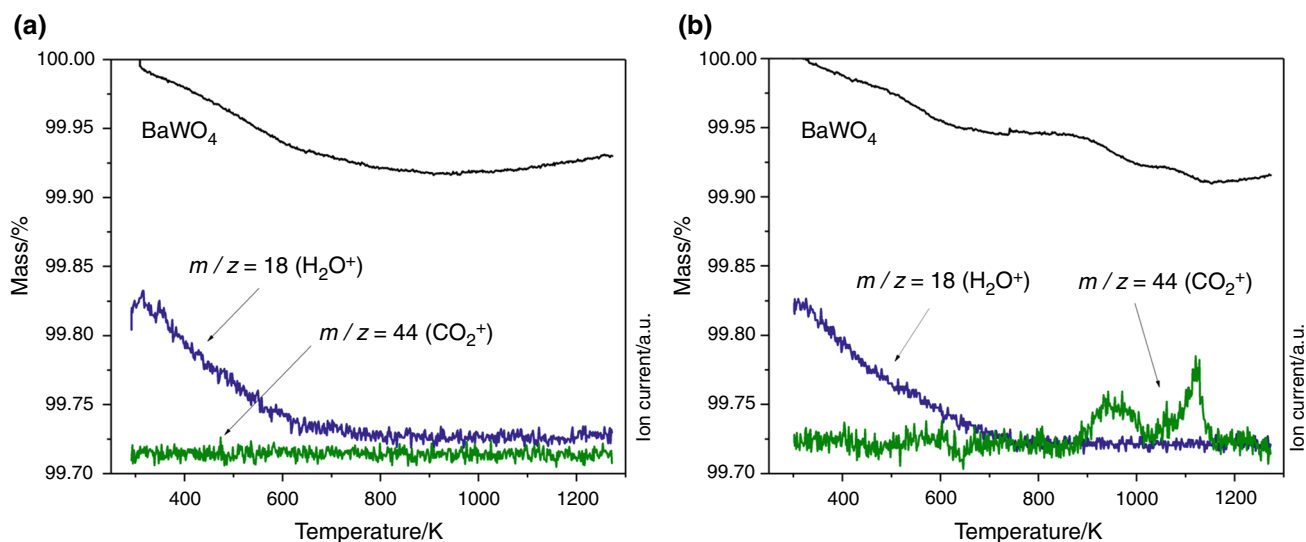
Fig. 3 TG curves and $m/z = 18$ and $m/z = 44$ ion current lines of $BaWO_4$ thermal degradation before (**a**) and after (**b**) the exposition test

for the second step is in the proportion about 2:1. Thus, it suggests that formation of non-crystalline barium carbonate is more favourable during the low-temperature exposition. It must be noticed that application of XRD method while the chemical stability of $BaWO_4$ in carbon dioxide and water vapour is evaluated is practically exclude as the amount of $BaCO_3$ in the sample after the exposition test is small and the carbonate can be partially amorphous. It should be mentioned that materials with scheelite-type structure are considered as chemically stable; however, presented data imply slight instability of $BaWO_4$ in CO_2 atmosphere. Thus, the effect of Nb-doping on materials chemical stability was also analysed.

Figure 4 shows TG curves for un-doped and Nb-doped $BaWO_4$ materials before and after the test. Before the exposition, there are no significant differences between the samples and the only effect seen on TG curve is the dehydration. The minor variation in the TG curves shape can only be the result of different amount of bonded water. As was previously discussed, un-doped $BaWO_4$ shows slight instability in CO_2 atmosphere. All doped materials, single and two phases, are chemically stable. They do not undergo reaction with carbon dioxide, as there is no mass loss in the temperature range corresponding to $BaCO_3$ thermal decomposition. The slight difference between the TG curves is the result of various amounts of water absorbed in the samples. It should be underlined that introduction of niobium into $BaWO_4$ structure results in a change in the materials chemical composition and leads to chemical stability improvement. The comparison of TG curves for un-doped $BaWO_4$, doped $BaWO_4$ (0.5Nb_BaWO_4) and samples with the highest niobium content (2Nb_BaWO_4, 5Nb_BaWO_4) indicates also that

for two-phase materials the partial incorporation of niobium into $BaWO_4$ structure occurs. Additionally, the good chemical stability of 2Nb_BaWO_4 and 5Nb_BaWO_4 samples implies that the second phase ($Ba_5Nb_4O_{15}$) is also chemically stable in CO_2- and water vapour-rich atmosphere. It must be noticed that the microstructure of un-doped and doped materials does not show significant differences and is not the factor limiting the chemical stability of analysed materials. Moreover, it can be postulated that incorporation of niobium into the barium tungstate structure leads to the chemical stability improvement in materials based on $BaWO_4$.

Electrical properties

According to the literature, $BaWO_4$ shows the oxide ion conductivity, similar to acceptor-doped $BaWO_4$ (doped with cesium into barium position) [27]. For $Ba_5Nb_4O_{15}$, proton and electron conductivity was observed for wet nitrogen and dry air atmosphere, respectively [34]. For evaluation of electrical properties of synthesised materials, un-doped $BaWO_4$, single-phase Nb-doped $BaWO_4$ (0.5Nb_BaWO_4) and two-phase material with the highest content of the second-phase $Ba_5Nb_4O_{15}$ (5Nb_BaWO_4) were chosen.

In Fig. 5, total electrical conductivity of $BaWO_4$-based materials is presented in Arrhenius coordinates. Measurements were taken for the temperature range 798–973 K. The electrical conductivity of un-doped $BaWO_4$ changes from $6.1 \cdot 10^{-10}$ Ω^{-1} cm^{-1} for 798 K to $9.2 \cdot 10^{-10}$ Ω^{-1} cm^{-1} for 973 K. For the entire analysed temperature range, the total conductivity of single-phase Nb-doped $BaWO_4$ (0.5Nb_BaWO_4) and two-phase material (5Nb_BaWO_4) is
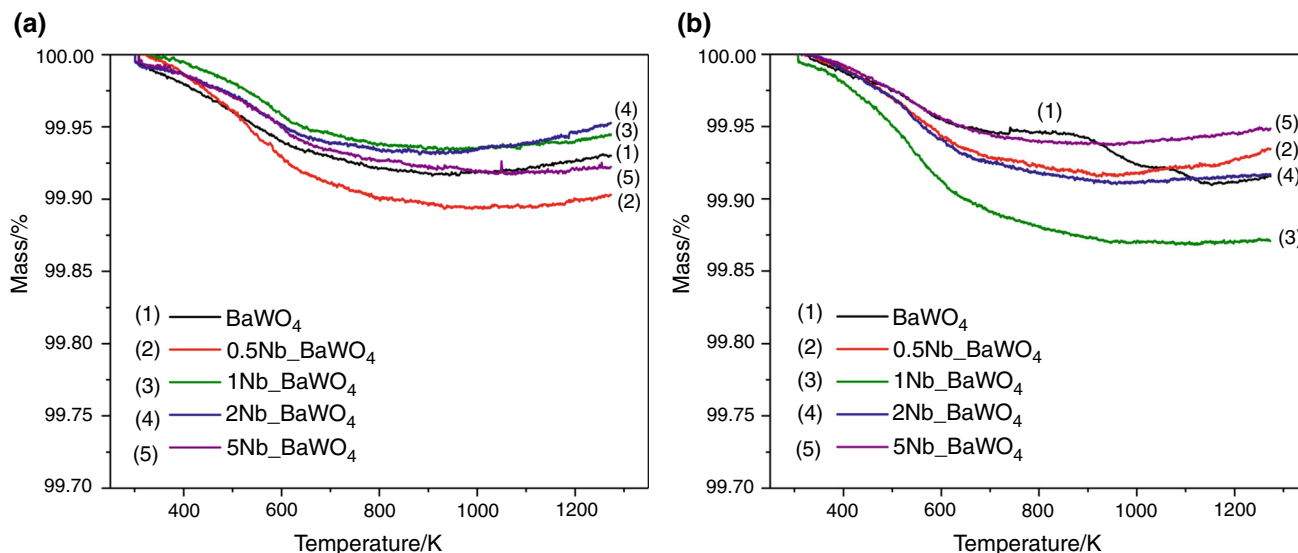
(a)

(b)

Fig. 4 TG curves of thermal degradation of $BaWO_4$-based materials before (**a**) and after (**b**) the exposition test

higher than for un-doped $BaWO_4$. Thus, incorporation of niobium into $BaWO_4$ scheelite structure leads to an increase in the total electrical conductivity, same as the presence of $Ba_5Nb_4O_{15}$ with hexagonal perovskite-related one.

Based on the Arrhenius plots, the activation energy of conductivity was calculated and is collected in Table 2. Calculated activation energy of $BaWO_4$ conductivity (1.06 ± 0.04 eV) stays in good agreement with values reported for this material previously (about 0.9 eV) [27] and suggests that conductivity is the result of oxide ion transport via the oxide ion vacancies, as this value is comparable to the activation energies of others oxide-ionic conductors [35]. The activation energy of conductivity for single-phase Nb-doped $BaWO_4$ (0.5Nb_BaWO_4) is lower

than for un-doped $BaWO_4$; however, it still corresponds to the value describing the oxide ion transport. It must be mentioned that incorporation of acceptor dopant (Nb^{5+}) into tungsten position in $BaWO_4$ structure should lead to formation the oxygen vacancies. Thus, the changes in the barium tungsten structure can result in a decrease in the E_a of conductivity and the higher concentration of oxygen vacancies can lead to an increase in total conductivity of Nb-doped $BaWO_4$ in comparison with un-doped $BaWO_4$. The activation energy of conductivity for material with the highest niobium content (5Nb_BaWO_4) is 1.40 ± 0.02 eV. It should be noticed that observed value of activation energy of conductivity in 5Nb_BaWO_4 material is the resultant value of conductivity of doped-$BaWO_4$ and Ba_5-Nb_4O_{15} as the 5Nb_BaWO_4 sample is two-phase material. The increase in E_a for two-phase material compared to single-phase $BaWO_4$ and 0.5Nb_BaWO_4 can be the result of the presence of second phase ($Ba_5Nb_4O_{15}$) located probably in the intergranular voids. According to the literature, $Ba_5Nb_4O_{15}$ shows in air the electron conductivity [34]. Thus, the presence of phase shows that the electron conductivity in the oxide ion conductor can result in blocking effect and lead to an increase in the observed value of activation energy of total conductivity.
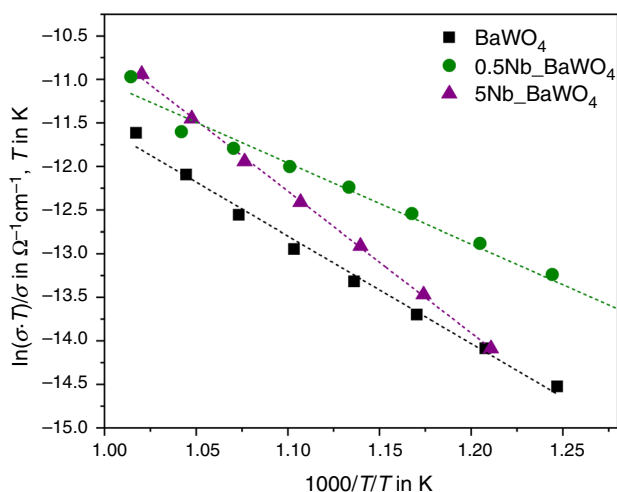

Fig. 5 Electrical conductivity of $BaWO_4$-based samples in Arrhenius coordinates

Table 2 Activation energies E_a/eV determined from DC measurements for $BaWO_4$-based materials

	$BaWO_4$	0.5Nb_BaWO_4	5Nb_BaWO_4
E_a of conductivity/ eV	1.06 ± 0.04	0.80 ± 0.03	1.40 ± 0.02

Analogous DC measurements were also taken for 1Nb_BaWO$_4$ material. The activation energy of conductivity determined based on Arrhenius plot was 1.57 ± 0.04 eV. This value is comparable with E_a of conductivity for 5Nb_BaWO$_4$ material and implies that for 1Nb_BaWO$_4$ material the blocking effect of second phase is also observed. It suggest that solubility limit of niobium in the BaWO$_4$ structure is in the range 0.5–1 mol%, similar as it was proposed based on the analysis of lattice parameters. However, it must be noticed that further investigations of electrical properties of acceptor-doped BaWO$_4$ together with the comprehensive analysis of its defect structure are necessary for the detailed analysis of conduction mechanism in doped BaWO$_4$ system.

Summary

Solid-state reaction method was applied to synthesise acceptor-doped barium tungstate. 0.5 mol% of niobium was introduced into tungsten position in tetragonal BaWO$_4$ with scheelite–type structure. For higher assumed Nb content (1.0, 2.0 and 5.0 mol%), the formation of second phase—Ba$_5$Nb$_4$O$_{15}$—was observed or postulated. Thus, the solubility limit of niobium in BaWO$_4$ structure was found in the range 0.5–1 mol%. However, partial incorporation of niobium into tungsten position in BaWO$_4$ structure is observable also for materials with higher niobium content. The grain size for all synthesised materials was 20–50 µm and was independent of the dopant amount. However, dopant addition led to a decrease in the volume fraction of close porosity and better sinterability of BaWO$_4$-based materials.

The exposition test (long-term, low-temperature exposure to CO$_2$ and water vapour) was performed in order to determine the chemical stability of BaWO$_4$-based materials against the presence of carbon dioxide and water vapour. Thermal analysis was applied for this parameter evaluation, as comparison of mass loss for samples before and after the test was performed. Moreover, the total mass loss for samples after the test can be directly treated as the measure of chemical instability of materials in CO$_2$- and water vapour-rich atmosphere. It was shown that introduction of niobium into BaWO$_4$ structure improves the barium tungsten chemical stability. Moreover, it was observed that the Ba$_5$Nb$_4$O$_{15}$ phase is also chemically stable in the applied conditions.

Electrical properties of synthesised materials were characterized by DC electrical conductivity measurements. The effect of incorporated niobium and the presence of Ba$_5$Nb$_4$O$_{15}$ phase on the electrical properties of BaWO$_4$-based materials was observed. The values of activation energy imply the domination of oxide ion conductivity;
however, further investigations are required for description of conductivity mechanism in Nb-doped BaWO$_4$ system.

References

1. Sun L, Cao M, Wang Y, Sun G, Hu C. The synthesis and photoluminescent properties of calcium tungstate nanocrystals. J Cryst Growth. 2006;289:231–5.
2. Cavalcante LS, Longo VM, Sczancoski JC, Almeida MAP, Batista AA, Varela JA, Orlandi MO, Longo E, Li S. Electronic structure, growth mechanism and photoluminescence of CaWO$_4$ crystals. CrystEngComm. 2012;14:853–68.
3. Abreu MFC, Motta FV, Lima RC, Li MS, Longo E, Marques APDA. Effect of process parameters on photophysical properties and barium molybdate phosphors characteristics. Ceram Int. 2014;40:6719–29.
4. Brazdil JF. Scheelite: a versatile structural template for selective alkene oxidation catalysts. Catal Sci Technol. 2015;5:3452–8.
5. Chen W, Inagawa Y, Omatsu T, Tateda M, Takeuchi N, Usuki Y. Diode-pumped, self-stimulating, passively Q-switched Nd^{3+}: PbWO$_4$ Raman laser. Opt Commun. 2001;194:401–7.
6. Takai S, Sugiura K, Esaka T. Ionic conduction properties of Pb$_{1-x}$M$_x$WO4 + δ (M = Pr, Tb). Mater Res Bull. 1999;34:193–202.
7. Krzmanc MM, Logar M, Budic B, Suvorov D. Dielectric and microstructure study of the SrWO$_4$, BaWO$_4$ and CaWO$_4$ scheelite ceramics. J Am Ceram Soc. 2011;94:2464–72.
8. Jena P, Nallamuthu N, Hari Prasad K, Venkateswarlu M, Satyanarayana N. Structural characterization and electrical conductivity studies of BaMoO$_4$ nanofibers prepared by sol–gel and electrospinning techniques. J Sol–Gel Sci Technol. 2014;72:480–9.
9. Cavalcante LS, Sczancoski JC, Lima LF Jr, Espinosa JWM, Pizani PS, Varela JA, Longo E. Synthesis, characterization, anisotropic growth and photoluminescence of BaWO$_4$. Crys Growth Des. 2009;9:1002–12.
10. Tian G, Sheng N, Qiu X. Structure and photoluminescence properties of SrWO$_4$ 3D microspheres synthesized by the surfactant-assisted hydrothermal method. Cryst Res Technol. 2014;49:360–5.
11. Sczancoski JC, Bomio MDR, Cavalcante LS, Joya MR, Pizani PS, Varela JA, Longo E, Siu Li M, Andrés JA. Morphology and blue photoluminescence emission of PbMoO$_4$ processed in conventional hydrothermal. J Phys Chem. 2009;113:5812–22.
12. Thongtem T, Phuruangrat A, Thongtem S. Microwave-assisted synthesis and characterization of SrMoO$_4$ and SrWO$_4$ nanocrystals. J Nanopart Res. 2010;12:2287–94.
13. Thongtem T, Phuruangrat A, Thongtem S. Preparation and characterization of nanocrystalline SrWO$_4$ using cyclic microwave radiation. Curr Appl Phys. 2008;8:189–97.
14. Thongtem T, Phuruangrat A, Thongtem S. Characterization of MeWO$_4$ (Me = Ba, Sr and Ca) nanocrystallines prepared by sonochemical method. Appl Surf Sci. 2008;254:7581–5.
15. Porto SL, Longo E, Pizani PS, Boschi TM, Simoes LGP, Lima SJG, Ferreira JM, Soledad LEB, Espinoza JWM, Cassia-Santos MR, Maurera MAMA, Paskocimas CA, Santos IMG, Souza AG. Photoluminescence in the Ca$_x$Sr$_{1-x}$WO$_4$ system at room temperature. J Solid State Chem. 2008;181:1876–81.
16. Hallaoui A, Taoufyq A, Arab M, Bakiz B, Benlhachemi A, Bazzi L, Villain S, Valmalette J-C, Guinneton F, Gavarri J-R. Influence

of chemical substitution on the photoluminescence of $Sr_{(1-x)}Pb_xWO_4$ solid solution. J Solid State Chem. 2015;227:186–95.

17. Rendón-Angeles JC, Matamoros-Veloza Z, Gonzalez LA, López-Cuevas J, Ueda T, Yanagisawa K, Hernández-Calderón I, Garcia-Rocha M. Rapid hydrothermal synthesis of $SrMo_{1-x}W_xO_4$ powders: structure and luminescence characterization. Adv Powder Technol. 2017;28:629–40.

18. Sun XY, Sun XD, Li XG, He J, Wang BS. Synthesis and luminescence of $BaWO_4:Ln^{3+}$ (Ln = Eu, Tb, and Dy) powders. J Electron Mater. 2014;43:3534–8.

19. Priya A, Sinha E, Rout SK. Structural, optical and microwave dielectric properties of $Ba_{1-x}Sr_xWO_4$ ceramics prepared by solid state reaction route. Solid State Sci. 2013;20:40–5.

20. Culver SP, Greaney MJ, Tinoco A, Brutchey RL. Low-temperature synthesis of homogeneous solid solutions of scheelite-structured $Ca_{1-x}Sr_xWO_4$ and $Sr_{1-x}Ba_xWO_4$ nanocrystals. Dalton Trans. 2015;44:15042–8.

21. Piatkowska M, Tomaszewicz E. Synthesis, structure, and thermal stability of new scheelite-type $Pb_{1-3x}\square_xPr_{2x}(MoO_4)_{1-3x}(WO_4)_{3x}$ ceramic materials. J Therm Anal Calorim. 2016;126:111–9.

22. Łącz A, Pasierb P. Synthesis and properties of $BaCe_{1-x}Y_xO_{3-\delta}$–$BaWO_4$ composite protonic conductors. J Therm Anal Calorim. 2013;113:405–12.

23. Norby T. Solid-state protonic conductors: principles, properties, progress and prospects. Solid State Ion. 1999;125:1–11.

24. Thangadurai V, Knittlmayer C, Weppner W. Metathetic room temperature preparation and characterization of scheelite-type ABO_4 (A = Ca, Sr, Ba, Pb; B = Mo, W) powders. Mater Sci Eng B-Adv. 2004;106:228–33.

25. Esaka T. Ionic conduction in substituted scheelite-type oxides. Solid State Ion. 2000;136–137:1–9.

26. Esaka T, Tachibana R, Takai S. Oxide ion conduction in the Sm-substituted $PbWO_4$ phases. Solid State Ion. 1996;92:129–33.

27. Takai S, Morishita J, Kondo Y, Yao T, Yabutsuka T, Esaka T. Electrochemical properties of Cs-substituted $CaWO_4$ and $BaWO_4$ oxide ion conductors. J Ceram Soc Jpn. 2016;124:819–22.

28. Cheng J, Tian C, Zhao D. Synthesis and electrochemical properties of $Ca0.9La0.1WO4 + \delta$ Electrolyte for Solid Oxide Fuel Cells. J Solid State Electrochem. 2011;16:753–8.

29. Vigen CK, Haugsrud R. Proton Conductivity in Solid Solution $0.7(CaWO_4)$–$0.3(La_{0.99}Ca_{0.01}NbO_4)$ and $Ca_{(1-x)}La_xW_{(1-y)}Ta_yO_4$. J Am Ceram Soc. 2013;96:3812–20.

30. Shannon RD. Revised effective ionic radii and systematic studies of interatomic distances in halides and chalcogenides. Acta Crystallogr. 1976;32:751–67.

31. Ge WW, Zhang HJ, Wang JY, Liu JH, Xu XG, Hu XB, Jiang MH, Ran DG, Sun SQ, Xia HR, Boughton RI. Thermal and mechanical properties of $BaWO_4$ crystal. J Appl Phys. 2005;98:013542-1–6.

32. Russ JC, Dehoff RT. Practical stereology. 2nd ed. Berlin: Springer; 2000.

33. Galwey AK, Brown ME. Thermal decomposition of ionic solids. Amsterdam: Elsevier; 1999.

34. Zhao H, Feng S, Xu W, Shi Y, Mao Y, Zhu X. A rapid chemical route to niobates: hydrothermal synthesis and transport properties of ultrafine $Ba_5Nb_4O_{15}$. J Mater Chem. 2000;10:965–8.

35. Ling CD, Avdeev M, Kutteh R, Kharton VV, Yaremchenko AA, Fialkova S, Sharma N, Macquart RB, Hoelzel M, Gutmann M. Structures, phase transitions, hydration, and ionic conductivity of $Ba_4Nb_2O_9$. Chem Mater. 2009;21:3853–64.